ς ϟ⸗

REPORT DOCUMENTATION PAGE

1. REPORT DATE (DD-MM-YYYY)	2. REPORT TYPE		3. DATES COVERED (From - To)
13-02-2012	Journal Article		

4. TITLE AND SUBTITLE	5a. CONTRACT NUMBER
An Analysis of Diffuse Attenuation in the Northern Gulf of Mexico Hypoxic Zone Using the SeaWIFS Satellite Data Record	
	5b. GRANT NUMBER
	5c. PROGRAM ELEMENT NUMBER
	0601153N

6. AUTHOR(S)	5d. PROJECT NUMBER
B. Schaeffer, G. Sinclair, J. Lehrter, M. Murrell, J. Kurtz, Richard Gould, D. Yates, G. Smith	
	5e. TASK NUMBER
	5f. WORK UNIT NUMBER
	73-8782-09-5

7. PERFORMING ORGANIZATION NAME(S) AND ADDRESS(ES)	B. PERFORMING ORGANIZATION REPORT NUMBER
Naval Research Laboratory Oceanography Division Stennis Space Center, MS 39529-5004	NRL/JA/7330-10-0165

9. SPONSORING/MONITORING AGENCY NAME(S) AND ADDRESS(ES)	10. SPONSOR/MONITOR'S ACRONYM(S)
Office of Naval Research One Liberty Center 875 North Randolph Street, Suite 1425 Arlington, VA 22203-1995	ONR
	11. SPONSOR/MONITOR'S REPORT NUMBER(S)

12. DISTRIBUTION/AVAILABILITY STATEMENT

Approved for public release, distribution is unlimited.

20120217365

13. SUPPLEMENTARY NOTES

14. ABSTRACT

The Sea-viewing Wide Field-of-View Sensor (SeaWiFS) derived diffuse light attenuation along the Louisiana continental shelf (LCS) was examined at monthly scales from 1998 to 2007 to characterize temporal and spatial patterns, and responsible physical forcing conditions. The SeaWiFS diffuse light attenuation ranged from 0.10 to 2.64 m^{-1}. Stepwise multiple linear regression analysis suggested that spatial and temporal patterns in diffuse light attenuation were influenced by wind speed, nutrient loading, and river discharge from the Mississippi and Atchafalaya River Basin. SeaWiFS daily integrated surface photosynthetically active radiation (PAR, 400 -700 nm) and diffuse light attenuation were used to calculate the absolute PAR and percentage of surface PAR that reached the sediment water interface (SWI) on the LCS. Large portions of the LCS were euphotic to the SWI especially during April and May. This finding implied that significant primary production was possible beneath the pycnocline during spring and early summer. In addition, this study was the first to demonstrate that the euphotic depth was correlated to the depth at which the water column turned hypoxic on the LCS. The development of hypoxic waters may be influenced by decreased light availability below the pycnocline in addition to aforementioned physical forcing.

15. SUBJECT TERMS

SeaWiFS, light, attenuation, euphotic depth, Louisiana continental shelf, hypoxia

16. SECURITY CLASSIFICATION OF:			17. LIMITATION OF ABSTRACT	1B. NUMBER OF PAGES	19a. NAME OF RESPONSIBLE PERSON
a. REPORT	b. ABSTRACT	c. THIS PAGE	UU	10	Richard Gould
Unclassified	Unclassified	Unclassified			19b. TELEPHONE NUMBER (Include area code) 228-688-5587

An analysis of diffuse light attenuation in the northern Gulf of Mexico hypoxic zone using the SeaWiFS satellite data record

Blake A. Schaeffer [a,*], Geoffrey A. Sinclair [b], John C. Lehrter [a], Michael C. Murrell [a], Janis C. Kurtz [a], Richard W. Gould [c], Diane F. Yates [a]

[a] US EPA National Health and Environmental Effects Research Laboratory, Gulf Ecology Division, 1 Sabine Island Drive, Gulf Breeze, FL 32561, USA
[b] Louisiana Universities Marine Consortium, 8124 Highway 56, Chauvin, LA 70344, USA
[c] Bio-Optical Physical Processes and Remote Sensing Section, Code 7331, Naval Research Laboratory, Stennis Space Center, MS 39529, USA

ABSTRACT

The Sea-viewing Wide Field-of-View Sensor (SeaWiFS) derived diffuse light attenuation along the Louisiana continental shelf (LCS) was examined at monthly scales from 1998 to 2007 to characterize temporal and spatial patterns, and responsible physical forcing conditions. The SeaWiFS diffuse light attenuation ranged from 0.10 to 2.64 m^{-1}. Stepwise multiple linear regression analysis suggested that spatial and temporal patterns in diffuse light attenuation were influenced by wind speed, nutrient loading, and river discharge from the Mississippi and Atchafalaya River Basin. SeaWiFS daily integrated surface photosynthetically active radiation (PAR, 400–700 nm) and diffuse light attenuation were used to calculate the absolute PAR and percentage of surface PAR that reached the sediment water interface (SWI) on the LCS. Large portions of the LCS were euphotic to the SWI especially during April and May. This finding implied that significant primary production was possible beneath the pycnocline during spring and early summer. In addition, this study was the first to demonstrate that the euphotic depth was correlated to the depth at which the water column turned hypoxic on the LCS. The development of hypoxic waters may be influenced by decreased light availability below the pycnocline in addition to aforementioned physical forcing.

Published by Elsevier Inc.

1. Introduction

The Louisiana continental shelf (LCS) is strongly influenced by the discharge of the Mississippi and Atchafalaya River Basin (MARB). Nutrient-rich water is delivered to the LCS through the MARB, with maximum concentrations occurring in the spring. Two thirds of the Mississippi River flow enters the Gulf of Mexico through the Mississippi River bird-foot delta, whereas the remaining third is delivered from the Atchafalaya River (Dale et al., 2010). Historical records indicate that nutrient concentrations in the Mississippi River increased approximately 2-fold during a 25-year period beginning in the mid-1950s (Goolsby et al., 2001). However, there was no significant change in river nutrient concentrations from 1979 to 2007 (Greene et al., 2009).

River nutrient loading increases primary productivity, phytoplankton biomass and therefore organic matter within the river plume and adjacent coastal waters (Lohrenz et al., 1997, 2008; Turner & Rabalais, 1991). The effects of nutrient enhanced productivity across the shelf region have been inferred from modeling (Bierman et al., 1994; Justic et al., 1996; Scavia et al., 2003) and by sediment geochemical measures (Eadie et al., 1994; Rabalais et al., 2004, 2007; Turner et al., 2004). The

transport and downward flux of organic matter to the sub-pycnocline waters is believed to fuel microbial metabolism that consumes oxygen, thus contributing to hypoxic conditions below the pycnocline (Redalje et al., 1994; Wysocki et al., 2006). This net oxygen consumption contributes to the largest zone of oxygen-depletion in the United States coastal waters, averaging 13,800 km^2 between 1985 and 2008 based on annual July surveys (http://gulfhypoxia.net).

The net consumption of oxygen in below-pycnocline waters and the sediments is the primary cause of hypoxia. Potential mechanisms offsetting oxygen consumption below the pycnocline are processes such as lateral and vertical oxygen flux, and in situ oxygen production via light driven photosynthesis (Justic et al., 1996; Lehrter et al., 2009). Light below the pycnocline can support both phytoplankton and the microphytobenthic (MPB) net production. MPB assemblages can persist at light levels as low as 0.1% surface irradiance (Cahoon, 1999), whereas phytoplankton typically become light-limited at 1% of surface irradiance (Kirk, 1994). While diffuse light attenuation is high within the Mississippi River plume (Lohrenz et al., 1999), it decreases with increasing salinity such that large portions of the LCS, where hypoxia occurs, are euphotic throughout the water column and to the sediment water interface (SWI) (Lehrter et al., 2009). The Bierman et al.'s (1994) deterministic mass balance model suggests that light penetrating below the pycnocline is an important factor influencing organic matter production and dissolved oxygen concentrations. Dortch et al. (1994) estimated

* Corresponding author. Tel.: + 1 850 934 9205; fax: + 1 850 934 2401.
E-mail address: schaeffer.blake@epa.gov (B.A. Schaeffer).

that photosynthesis at the sediment–water interface contributed up to 57% of the lower water column photosynthesis. In this respect, an increased understanding of light availability on the LCS is critical to understanding the relative contributions of water column and SWI photosynthesis to the supply of carbon and oxygen in the hypoxic zone.

In this paper we examine shelf-wide synoptic estimates of diffuse light attenuation, absolute daily integrated photosynthetically active radiation (PAR, 400–700 nm), and the percentage of daily integrated PAR at the SWI using satellite observations. We characterize the timing, location, and physical forcing impacts on diffuse light attenuation and PAR reaching the SWI. While surface PAR and diffuse light attenuation on the LCS are routinely measured through a variety of ship-based surveys, these observations are typically limited to a few stations per day spatially and only a few weeks at a time temporally. In addition, field surveys in the northern Gulf of Mexico are biased towards the spring and summer months when hypoxia is prevalent. Therefore field observations are inadequate to fully describe water column diffuse light attenuation across the entire LCS over the entire annual cycle. In contrast, satellite-derived data provide synoptic coverage, once properly validated against shipboard or buoy observations. The goals of this study are: (1) validate the Sea-viewing Wide Field-of-View Sensor (SeaWiFS) daily integrated surface PAR, (2) adjust the SeaWiFS Kd_{490} diffuse light attenuation coefficient product to represent Kd_{PAR} with field observations of Kd_{PAR}, (3) estimate the spatial and temporal patterns of absolute and percentage surface PAR at the SWI, (4) interpret how the euphotic depth relates to hypoxia, and (5) examine relationships between SeaWiFS diffuse light attenuation and wind speed, MARB discharge, and nutrient loading from 1998 to 2007.

2. Methods

Field observations were used from EPA Gulf Ecology Division shelf-wide surveys (Fig. 1), Louisiana Universities Marine Consortium (LUMCON) July surveys (Fig. 1, unpublished data, NOAA NODC, www.nodc.noaa.gov), and the LUMCON Lake Pontchartrain station (Fig. 1).

2.1. EPA Gulf Ecology Division field observations

Seven research cruises were conducted from 2005 to 2007 on the LCS where hypoxia routinely occurs (Fig. 1). Three cruises were conducted in the spring (March 2005, April 2006, and April 2007) and 4 cruises were conducted during summer months (September 2005, June 2006, September 2006, and August 2007). The March 2005 cruise was aboard the R/V *Longhorn* and the remaining cruises were aboard EPA's Ocean Survey Vessel *Bold*. With the exception of the September 2005 cruise, a Sea-Bird 911 CTD (Sea-Bird Electronics, Bellvue, WA, USA) was deployed to measure vertical profiles of temperature, salinity, dissolved oxygen, and photosynthetically active radiation (PAR, Biospherical Instruments, QSP-200, San Diego, CA, USA). A Sea-Bird 43 dissolved oxygen sensor on the CTD was used to estimate the depth at which the water column turned hypoxic (defined as <2 mg O_2 L^{-1}, 1.4 ml O_2 L^{-1}, or ~62 O_2 µmol kg^{-1}). Secchi depth was recorded at each station occupied during daylight hours.

Surface PAR (400–700 nm) (E_0) was measured continuously with a 2π LI-COR LI-190 irradiance sensor and averaged at 15 min intervals. The diffuse light attenuation coefficient (Kd_{PAR}, m^{-1}) determined from the CTD was calculated as the slope of $\ln(E_z/E_0)$ versus depth (z) where E_z was the PAR at depth z and E_0 was the PAR measured at the surface. The reciprocal of Secchi depth (SD) was regressed against Kd_{PAR} at Gulf Ecology Division sites. The regression coefficients were then used to estimate Kd_{PAR} at all LUMCON sites.

2.2. LUMCON field observations

Secchi depth was used to estimate diffuse light attenuation coefficients during LUMCON surveys because PAR measurements were not reported at LUMCON sites. SeaWiFS surface daily integrated PAR
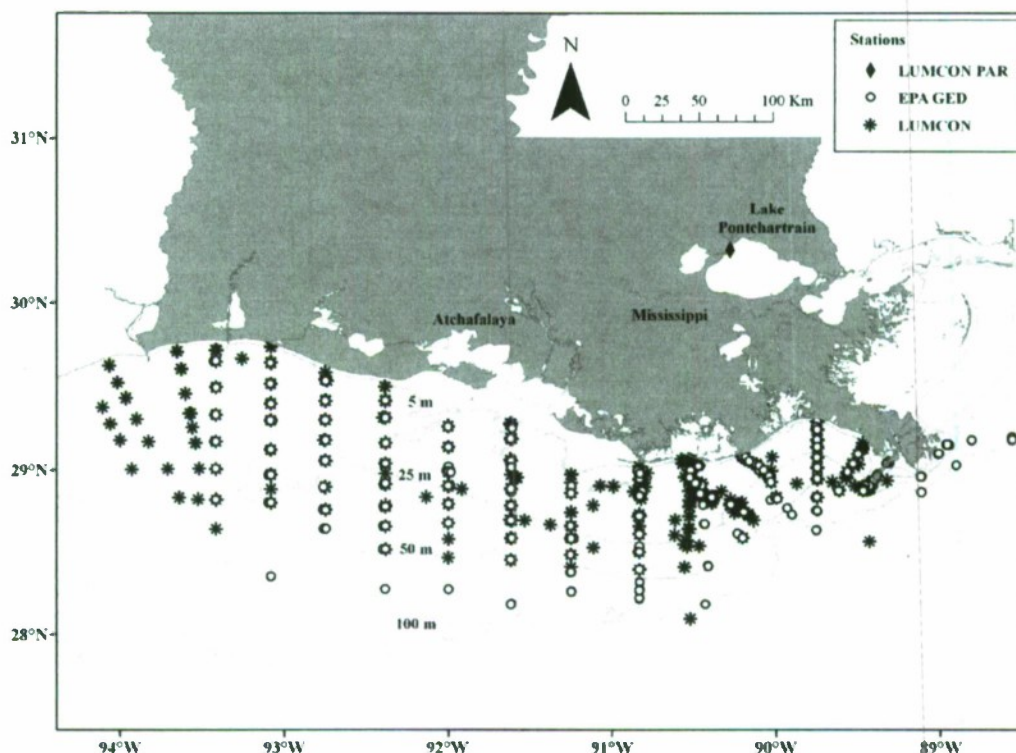

Fig. 1. Map of study region in the northern Gulf of Mexico. Locations of all EPA Gulf Ecology Division (GED) sample stations are indicated in open circles, LUMCON sample stations are indicated with asterisks, and the LUMCON Lake Pontchartrain monitoring station is indicated as a diamond.

(Frouin et al., 2003) was validated against the LUMCON Lake Pontchartrain environmental monitoring station (Fig. 1) retrieved on January 2009 from the archive data site at http://weather.lumcon.edu/archivedata/select.asp. The monitoring station PAR sensor was calibrated every 2 years and serviced every other month with periods of monthly servicing. Instantaneous PAR was averaged hourly at the station and integrated throughout each day from 2001 to 2007 using Interactive Data Language (IDL, ITT VIS). Data for daily integration from 2004 were not available at the Lake Pontchartrain station. LUMCON dissolved oxygen measurements were made with a Hydrolab Surveyor 3 (unpublished data, NOAA NODC) and was used to estimate the depth at which the water column turned hypoxic.

2.3. SeaWiFS satellite observations

Satellite ocean color data were obtained from the National Aeronautics and Space Administration (NASA) Ocean Color Web (Feldman & McClain, 2008). SeaWiFS provided daily images with pixels having a nominal 1.1 km spatial resolution when not obstructed by cloud cover. Atmospheric correction algorithms applied by NASA's fifth (5.2) SeaWiFS reprocessing included the standard near-infrared (NIR) correction for coastal waters (Arnone et al., 1998; Stumpf et al., 2003). SeaWiFS Data Analysis System (SeaDAS) version 5.3 (Baith et al., 2001) was used to process data from SeaWiFS level-1 to level-2 one-day images for comparison against field observation data. A 3×3 pixel box was used for each corresponding station latitude and longitude coordinate as described in Bailey and Werdell (2006). Satellite match-ups for validation of PAR and diffuse light attenuation were evaluated with a Model II geometric mean linear regression (Laws & Archie, 1981) using only in situ data collected between 10:00 and 14:00 local time on the same day as the satellite overpass. Monthly composites were temporal averages of flag-free pixels in each month from January 1998 through December 2007. Monthly composites were processed with the Naval Research Laboratory's Automated Processing System (APS) (Martinolich, 2005). SeaWiFS imagery covered between 27.15 to 30.40° N and 88.22 to 94.45° W.

Kd_{490} (Lee et al., 2005) was adjusted to represent Kd_{PAR} using the slope and intercept of an empirical regression between Kd_{PAR} field observations and the SeaWiFS Kd_{490} product. The exponential light extinction equation

$$E_z = E_0 * e^{(-Kd*z)}$$

was used to calculate the absolute and percentage of surface PAR at the SWI, and the depth of the euphotic layer, where E_z was the calculated light at the SWI, E_0 was SeaWiFS daily integrated surface PAR, Kd was the SeaWiFS $Kd_{490-PAR}$, and z was the depth of the SWI.

2.4. QuickScat wind

Wind speed data were obtained from the Physical Oceanography Distribution Active Archive Center (PO.DAAC) Ocean Earth Science Information Partner (ESIP) Tool (POET) with the Quick Scatterometer (QuickScat) from 27.15 to 30.40° N and 88.22 to 94.45° W. QuickScat measures wind speed of 3 to 20 m s^{-1} with an estimated accuracy of 2 m s^{-1} and vector resolution of 25 km (JPL, 2001). Monthly composites were compiled from January 2000 through December 2007.

2.5. Bathymetry, river discharge, and nutrient loads

Bathymetry data were obtained from the National Geophysical Data Center (NGDC Coastal Relief model, retrieved on May 2009 from www.ngdc.noaa.gov/mgg/coastal/coastal.html). The native resolution was 3 arc sec (~0.1 km), so the grid was resized to match 1 km resolution of the satellite imagery. The offshore boundary for

the domain was the 70 m isobath. Monthly average river discharge and nutrient loads were obtained from the USGS (http://toxics.usgs.gov/hypoxia/mississippi/nutrient_flux_yield_est.html).

A stepwise multiple linear regression analysis was used to determine if river discharge, nutrient concentration, and wind speed were important parameters in Kd interannual variability. The analysis equation was:

$$Kd = Wind + Q + Q.1 + Q.2 + NOx + NOx.1 + NOx.2 + Q:NOx$$
$$+ Q.1:NOx.1 + Q.2:NOx.2$$

where Q was the river discharge, Q.1 and Q.2 were the one and two-month lagged discharges, NOx was the nitrate concentration in the river, NOx.1 and NOx. 2 were the one and two-month lagged concentrations, and Q:NOx terms were the interaction terms.

Four alternate future scenarios were used to predict change in diffuse attenuation coefficients within each region from the stepwise multiple linear regression analysis. Scenarios were selected from Greene et al. (2009) to forecast changes based on suggested nutrient management strategies (Mississippi River/Gulf of Mexico Watershed Nutrient Task Force, 2001, 2008) and global climate change scenarios (Miller & Russell, 1992; Nijssen et al., 2001; Wolock & McCabe, 1999). Scenarios included (1) 30% and (2) 50% reduction in May NOx concentration with no change in May discharge, (3) 20% increase in May NOx, and (4) 20% increase in May discharge.

3. Results

3.1. Algorithms

There were 1257 paired observations from the LUMCON Lake Pontchartrain environmental monitoring station and the SeaWiFS imagery taken from 2001 through 2007. The paired observations were randomly divided so half of the data were used to develop regression coefficients and the other half of the data were used to validate the regression analysis. There was a significant positive correlation between SeaWiFS surface daily integrated PAR and LUMCON Lake Pontchartrain surface daily integrated PAR (Fig. 2, slope = 0.91, $R^2 = 0.72$, p<0.01, N = 631). Observed and predicted values of surface PAR agreed well and explained 90% of the variance of the validation data set (data not shown, slope = 1.10, $R^2 = 0.90$, p<0.01, N = 626). Therefore the regression coefficients from Fig. 2 were used to correct satellite-derived daily integrated PAR for LCS analysis. The regression of Gulf Ecology Division Kd_{PAR} versus 1/SD (Fig. 3) resulted in a slope of 1.44 ($R^2 = 0.94$, p<0.01). Of the 1115 in situ measurements from LUMCON there were 137 match-ups with SeaWiFS on the same day. Of the 374 in situ measurements from Gulf

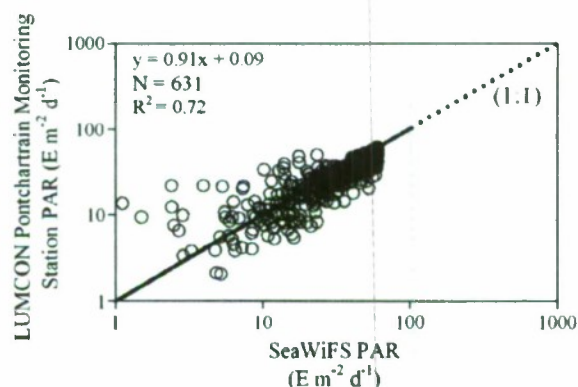
Fig. 2. Model II geometric mean linear regression of daily integrated surface PAR from the LUMCON Lake Pontchartrain monitoring station and SeaWiFS flag free pixels from 2001 through 2007. The dashed line represents the one to one fit.

Ecology Division there were 10 match-ups with SeaWiFS. The 147 paired observations from LUMCON and Gulf Ecology Division were randomly divided so half of the data were used to develop regression coefficients and the other half of the data were used to validate the regression analysis. LUMCON field measurements of Kd_{PAR} ranged from 0.05 to 14.4 m^{-1} with a mean of 0.69 ± 1.01 S.D. Gulf Ecology Division field measurements of Kd_{PAR} ranged from 0.03 to 7.2 m^{-1} with a mean of 0.48 ± 0.65 S.D. The regression between SeaWiFS Kd_{490} versus combined Gulf Ecology Division Kd_{PAR} and LUMCON Kd_{PAR} was significant (Fig. 4, slope = 1.07, $R^2 = 0.65$, p < 0.01, N = 68). Observed and predicted values of diffuse attenuation coefficients were in reasonable agreement and explained 68% of the variance (data not shown, slope = 1.07, $R^2 = 0.68$, p < 0.01, N = 79). The regression coefficients from Fig. 4 were used to adjust SeaWiFS Kd_{490} to represent Kd_{PAR} hereafter referred to as $Kd_{490-PAR}$.

3.2. Spatial, seasonal, and interannual patterns

The LCS was divided into five discrete regions (Fig. 5), to assist in spatial descriptions. The percent frequency of PAR > 1% at the SWI for March, April, and May, from 1998 through 2007, was used to guide regional divisions because this was the time of year when hypoxia begins to develop. Regional boundaries were drawn based on the visible spatial patterns in Fig. 5. Regions were ordered in decreasing values of average $Kd_{490-PAR}$ and increasing average water depth. The outer portion of the domain was restricted to the 70 m isobath. Region area, volume, and depth were reported in Table 1. The shallowest mean depth was in Region 1 (R1) and the euphotic depth reached the SWI <5% of the time during the spring months. Region 2 (R2) was just south of Atchafalaya Bay and the euphotic depth reached the SWI >50% of the time. Region 3 (R3) was drawn with the northern extent along the 10 m isobath and the euphotic depth reached the SWI between 0 and 40% of the time during the spring season. Region 4 (R4) was located adjacent to the Mississippi River, Barataria Bay, and Terrebonne Bay, and the euphotic depth reached the SWI <5% of the time. Finally, Region 5 (R5) had the 70 m contour along its southern most extent. Based on all years of ship observations, R5 was characterized by the highest salinity waters and the euphotic depth reached the SWI >50% of the time during March, April, and May.

$Kd_{490-PAR}$ 10-year monthly means (Fig. 6A) differed significantly between all regions for every month of the year (one-way ANOVA, p < 0.0001), with one exception. $Kd_{490-PAR}$ was not different significantly between R3 and R4 in February (one-way ANOVA, p = 0.91). $Kd_{490-PAR}$ increased significantly from May to June (one-way ANOVA, p < 0.001) and decreased from July to August (p < 0.001) in all regions. R1 mean $Kd_{490-PAR}$ was highest followed by R2, R3, R4, and R5 respectively. R1, R2, and R3 means $Kd_{490-PAR}$ peaked in
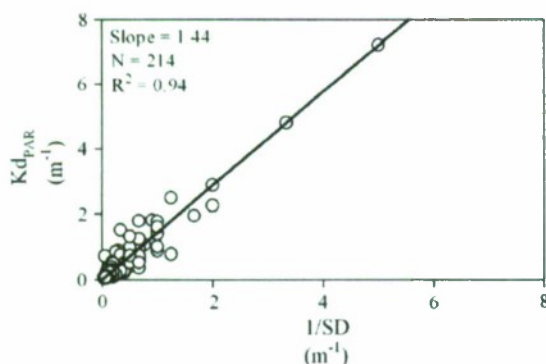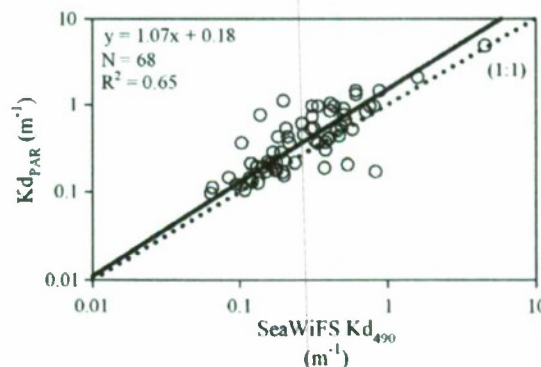

Fig. 4. Model II geometric mean linear regression of the SeaWiFS Kd_{490} diffuse light attenuation coefficient with LUMCON and Gulf Ecology Division Kd_{PAR}. The dashed line represents the one to one fit.

January while R4 and R5 means $Kd_{490-PAR}$ peaked in March and December, respectively. Minimum $Kd_{490-PAR}$ occurred in each region during the months of August or September. Seasonally, $Kd_{490-PAR}$ was greater in the winter than the summer in all regions. Percent (Fig. 6B) and absolute PAR (Fig. 6C) at the SWI was inversely proportional to the change in the $Kd_{490-PAR}$. Mean percent and absolute PAR at the SWI was lowest in the fall and winter, but peaked from April through September with a decrease in July. The lowest percent and absolute light at the SWI typically occurred in December and January. SeaWiFS daily integrated PAR (Fig. 6B) peaked between 50 and 60 E m^{-2} d^{-1} during June. MARB discharge (Fig. 6D) typically peaked in the spring and was at a minimum from August through October. Wind speed (Fig. 6D) was at a maximum during the winter months of November and December and at a minimum in July and August.

MARB discharge, total nitrogen concentration, and wind speed influences on $Kd_{490-PAR}$ were used to assess interannual variability (Table 2) and shorter time-scales during the months of May, June, and July (Table 3) when hypoxic conditions typically proliferate. The stepwise multiple linear regression analysis on the interannual scale (Table 2) indicated $Kd_{490-PAR}$ was correlated with wind speed in R5. Both wind speed and discharge were significantly related to $Kd_{490-PAR}$ in R1, R2, and R3. Discharge and NOx were the best predictors of $Kd_{490-PAR}$ in R4. $Kd_{490-PAR}$ during May, June, and July (Table 3) was mainly related to Q and NOx. For these months, $Kd_{490-PAR}$ had a significant negative correlation with wind speed in R5 and R4. Correlations among independent variables (co-linearity) may produce inaccurate estimates of regression coefficients, variability, and p-values (Kleinbaum et al., 1986). In this case, the lagged Q and lagged NOx were not strongly correlated, but literature provided minimal guidance on defining what level of correlation constituted a problem. Thus, only one Q and one NOx value was used. In cases where multiple lagged variables occurred, only the variable with the smallest p-value was retained.

The SeaWiFS derived euphotic depth correlated with the depth at which the water column turned hypoxic at <2 mg L^{-1} ($z_{Hypoxic}$), explaining 51% (p < 0.001) of the variability (Fig. 7A). Shallow euphotic depths occurred where there was shoaling of the hypoxic layer toward the surface, and deeper euphotic depths occurred where the hypoxic layer was closer to the SWI. Mean July $Kd_{490-PAR}$ within the maximal extent of the hypoxic zone (22,000 km^2 reported in 2002) was correlated to the normalized size of the July hypoxia area (Fig. 7B). The July hypoxic area size was normalized to the maximal extent of the hypoxic zone. Normalized hypoxic area increased with an increase in $Kd_{490-PAR}$. Percent surface PAR at the SWI was reported from monthly composites between 1998 and 2007 (Fig. 8). Mean percent PAR increased from January through May (Fig. 8A, B, C, D, and E) within all regions. R5 mean% PAR peaked in May while R2 and R3

Fig. 3. Model II geometric mean linear regression of the diffuse attenuation coefficient Kd_{PAR} determined from the Gulf Ecology Division CTD PAR data and inverse of Secchi depth.
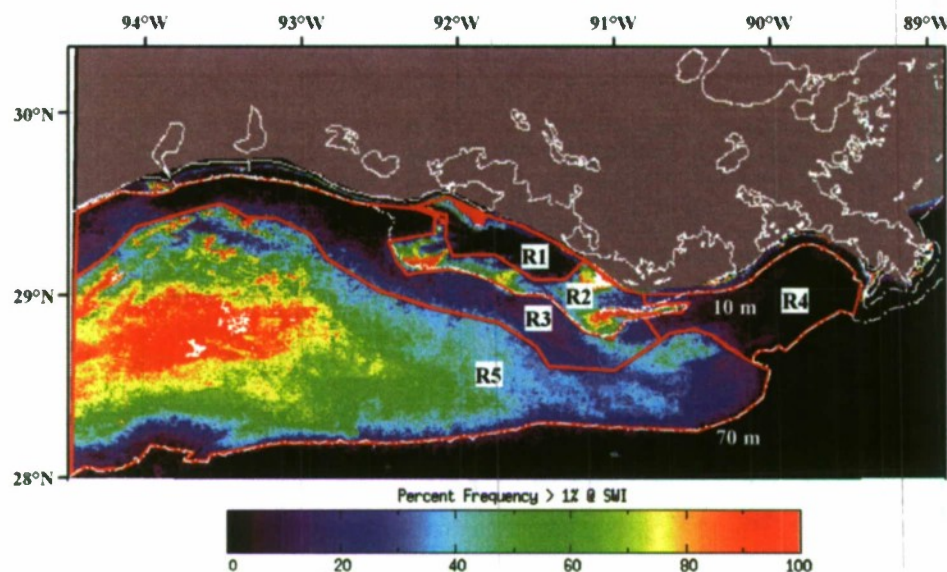
Fig. 5. Northern Gulf of Mexico regions based the spatial pattern of the percent frequency which the euphotic layer reaches the SWI for March, April, and May from 1998 through 2007. The domain of interest was within the 70 m isobaths. The 70 and 10 m isobaths are indicated as white broken lines.

peaked in August (Fig. 8H). R1 and R4 mean % PAR peaked in September (Fig. 8I). Mean percent PAR decreased in all regions from October (Fig. 8J) to November (Fig. 8K), with the lowest mean percent PAR reaching the SWI in December (Fig. 8L). Across our defined domain 46% of the area was greater than 0.1% PAR at the SWI and 2% of the area was greater than 1.0% PAR during January (Fig. 9). Ninety-four percent of the domain was greater than 0.1% PAR and 66% of the area was greater than 1.0% PAR during May. Finally, during July 90% of the domain was greater than 0.1% PAR and 36% of the area was greater than 1.0% PAR.

3.3. Future perspective

Generally, $Kd_{490-PAR}$ decreased under nitrogen reduction and increased under global climate change scenarios (Table 4). R4 was closest in proximity to the Mississippi River and had the largest relative percent change during all scenarios. R3 had the second largest percent decrease (-7% and -12%) under the 30% and 50% nitrogen reduction scenarios. R2 and R3 had identical increases of 5 and 6% during the increased nitrogen and discharge climate change scenarios. R1 $Kd_{490-PAR}$ had no change under any of the nitrogen reduction scenarios and increased 6% with increased discharge. Finally, R5 $Kd_{490-PAR}$ had no change under the increased discharge scenario, increased 3% with increased nitrogen, and decreased 5 and 8% with 30% and 50% nitrogen reduction.

Table 1
Area, volume, and depth statistics for regions 1 through 5.

Region	Area (km²)	Volume (×10⁶ km³)	Average depth (m)	Min depth (m)	Max depth (m)
R1	1992	9	4.5	1	7
R2	3065	19	6.2	1	16
R3	9334	135	14.5	3	30
R4	4343	123	28.4	7	70
R5	35,084	1293	36.8	7	75
Total	53,818	1579			

4. Discussion

4.1. SeaWiFS $Kd_{490-PAR}$ and PAR

Differences between the SeaWiFS Kd_{490} and Kd_{PAR} field observations were expected because Kd_{PAR} was the integral of the spectrum (400–700 nm) and Kd_{490} was a measure at a single waveband (Fig. 4). The PAR spectrum changed with depth in the water column due to different absorption rates at each wavelength. The red wavelengths attenuated rapidly with depth and the blue wavelengths penetrated deeper into the water column (Kirk, 1994). Differences between SeaWiFS PAR and the LUMCON Lake Pontchartrain PAR occurred because the SeaWiFS algorithm was calculated from a single instantaneous measurement per day (Frouin et al., 2003) and assumed cloud cover did not change throughout the day. The LUMCON PAR was influenced by changing cloud cover throughout the day.

Estimates of SeaWiFS $Kd_{490-PAR}$ assumed the diffuse light attenuation coefficient was constant throughout the water column. Inspection of Gulf Ecology Division CTD PAR profiles found 80% of vertical profiles had higher diffuse attenuation in the surface (unpublished data). Lugo-Fernandez et al. (2008) also reported higher diffuse attenuation in surface water which was typically over clearer Gulf of Mexico water. Jahnke et al. (2008) noted ship-based variations in diffuse attenuation measurements were biased toward calmer sea conditions potentially biasing benthic PAR estimates. The first optical depth observed by SeaWiFS, ranged from 0.27 to >13 m. The shallowest first optical depth occurred in R1 and the deepest first optical depth occurred in R5. The SeaWiFS data record provided the advantage of shelf-wide spatial coverage and long-term temporal measurements, which compensated for the inability of the satellite to measure $Kd_{490-PAR}$ throughout the water column to the SWI.

4.2. Spatial, seasonal, and interannual patterns in light attenuation

$Kd_{490-PAR}$ was highest in the late fall, winter, and early spring and lowest in the summer. This trend was consistent with Gulf Ecology Division and LUMCON field observations. At the interannual scale, patterns in $Kd_{490-PAR}$ co-varied with wind speed in all regions except R4 (Table 2). Previous studies of diffuse light attenuation on the LCS
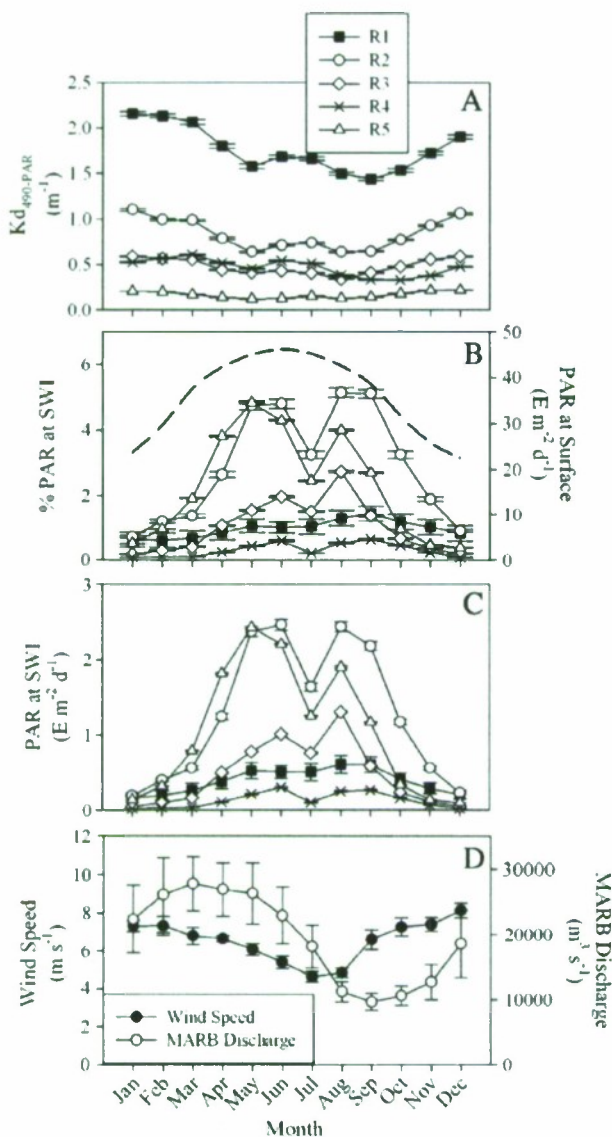
Fig. 6. Ten-year mean of SeaWiFS (A) $Kd_{490-PAR}$ (m^{-1}), (B) daily integrated surface PAR (E $m^{-2} d^{-1}$, black dashed line), % PAR (solid lines) at the SWI, and (C) absolute PAR at the SWI for all five regions each month of the year. Error bars indicate $2\times \pm$ SE. Eight year mean of (D) wind speed and MARB discharge.

Table 2

Multiple regression models for the response variable SeaWiFS Kd_{490} based on the 1998 to 2007 monthly averages of Kd_{490} for each region (R1, R2, R3, R4, and R5) and the independent variables: wind was the monthly average wind speed ($m s^{-1}$) for each region, Q was the monthly average combined discharge ($m^3 s^{-1}$) of the Mississippi and Atchafalaya Rivers and Q.1 and Q.2 were the one and two-month lagged average discharges, NOx was the flow-weighted mean monthly nitrate concentration for the combined Mississippi and Atchafalaya discharge and NOx.1 and NOx.2 were the one and two-month lagged average nitrate concentrations. df are degrees of freedom. β are the regression coefficients. Partial p-values are bold-italicized when significant at $\alpha = 0.05$.

Region	p-value	R^2	df	Variable	Beta	Partial p-value	Intercept
R1	1.1E-16	0.56	90	Wind	0.09	*<0.0001*	0.74
				Q	2.22E-05	*<0.0001*	
R2	2.2E-14	0.5	90	Wind	0.12	*<0.0001*	-0.008
				Q	5.05E-06	*0.01*	
R3	<1E-16	0.62	90	Wind	0.07	*<0.0001*	0.01
				Q	2.77E-06	*0.003*	
R4	<1E-16	0.57	90	Q	1.12E-05	*<0.0001*	0.24
				NOx.1	5.76E-04	*0.03*	
R5	5.8E-13	0.43	94	Wind	0.026	*<0.0001*	0.02

Table 3

Multiple regression models for the response variable SeaWiFS Kd_{490} based on the 1998 to 2007 May, June, and July averages of Kd_{490} for each region (R1, R2, R3, R4, and R5) and the independent variables: Wind was the monthly average wind speed ($m s^{-1}$) for each region, Q was the monthly average combined discharge ($m^3 s^{-1}$) of the Mississippi and Atchafalaya Rivers and Q.1 and Q.2 were the one and two-month lagged average discharges, NOx was the flow-weighted mean monthly nitrate concentration for the combined Mississippi and Atchafalaya discharge and NOx.1 and NOx.2 were the one and two-month lagged average nitrate concentrations. df are degrees of freedom. β are the regression coefficients. Partial p-values are bold-italicized when significant at $\alpha = 0.05$.

Region	p-value	R^2	df	Variable	Beta	Partial p-value	Intercept
R1	0.015	0.33	21	Wind	-0.08	0.22	1.63
				Q	2.18E-05	*0.005*	
R2	0.026	0.24	27	Q	8.28E-06	*0.01*	0.39
				NOx.2	1.49E-03	*0.04*	
R3	2.0E-04	0.61	20	Wind	0.02	0.24	0.12
				Q	6.12E-06	*0.0008*	
				NOx.2	9.86E-04	*0.002*	
R4	3.0E-04	0.6	20	Wind	-0.09	*0.002*	0.5
				Q	1.64E-05	*<0.0001*	
				NOx.2	1.76E-03	*0.005*	
R5	0.009	0.36	21	Wind	-0.01	*0.02*	0.21
				NOx.2	2.10E-04	0.11	

were limited both spatially and temporally making it difficult to infer the role of diffuse light attenuation in regulating both primary production and hypoxia across the shelf. Diffuse light attenuation coefficients reported previously (D'Sa & Miller, 2003; Lehrter et al., 2009; Lugo-Fernandez et al., 2008) were similar to the SeaWiFS $Kd_{490-PAR}$ values reported in this study throughout regions 2, 3, 4, and 5 (Fig. 6). Only Region 1, the shallow region adjacent to the Atchafalaya, had higher SeaWiFS $Kd_{490-PAR}$ (2.64 m^{-1}) than reported previously.

A conceptual explanation of the possible dynamics was developed, based on results presented here and previously published reports that
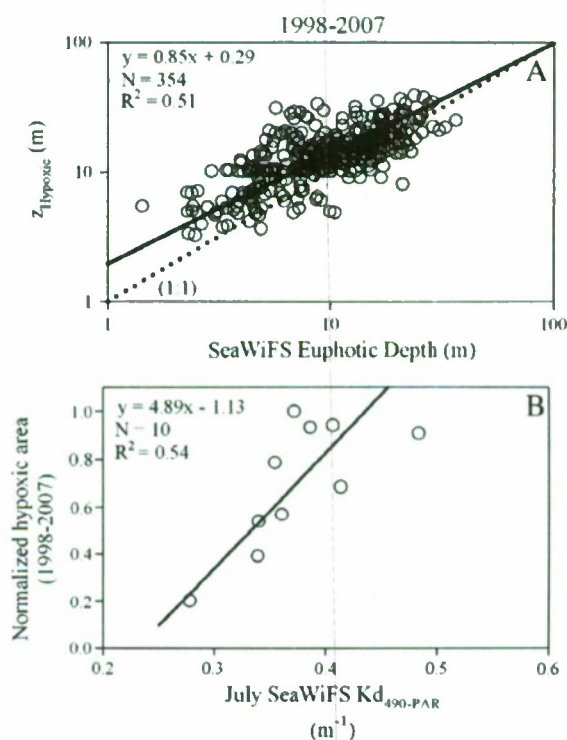

Fig. 7. Model II linear regressions of (A) euphotic depth estimated from SeaWiFS against the depth at which the water column turned hypoxic ($z_{Hypoxic}$, <2.0 mg L^{-1}), and (B) mean July $Kd_{490-PAR}$ within the maximal extent of the hypoxic area against the normalized hypoxic area reported for the month of July.
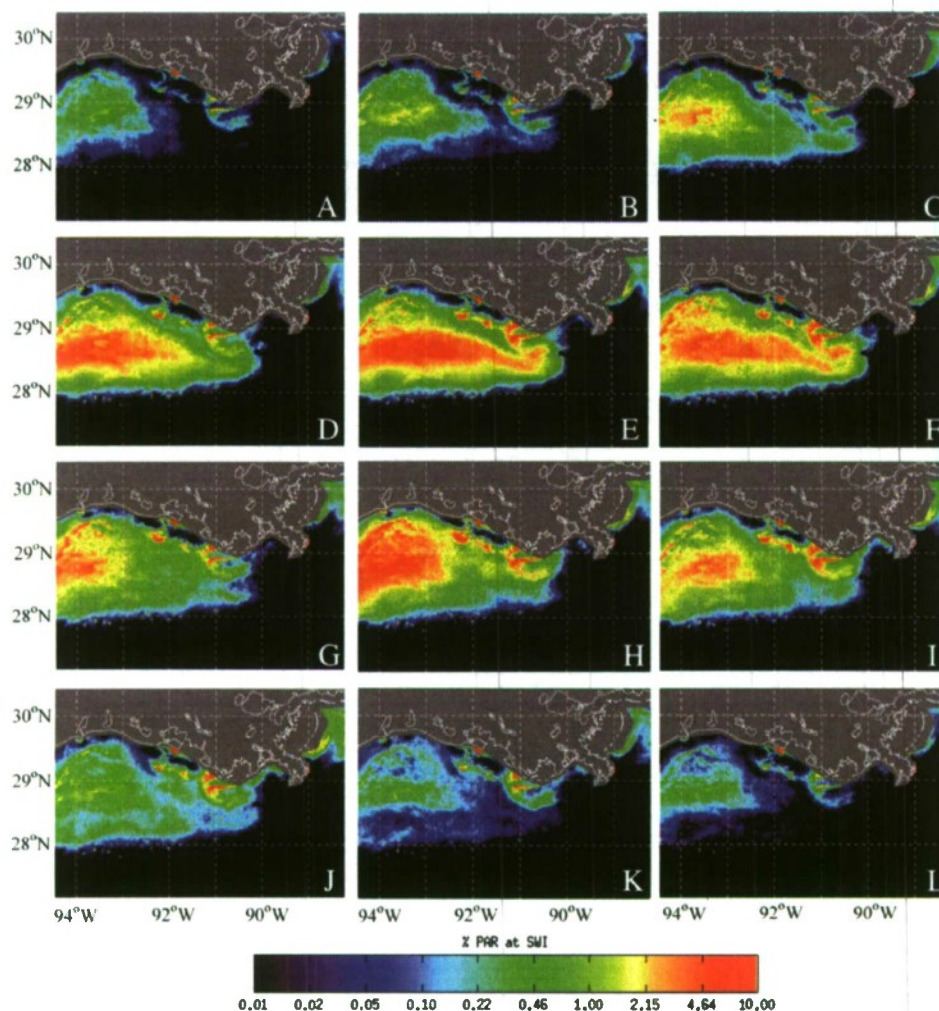
Fig. 8. Ten-year monthly average composites of SWI percent PAR for (A) January, (B) February, (C) March, (D) April, (E) May, (F) June, (G) July, (H) August, (I) September, (J) October, (K) November, and (L) December. A gray land mask covers coastal waters, such as the Atchafalaya, where SeaWiFS was not validated with field observations.

measured the individual light attenuating components. This study did not quantify individual light attenuating components. Diffuse light attenuation is the 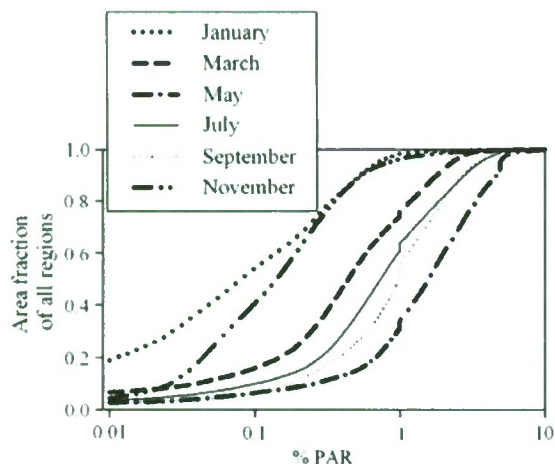sum of scattering and light absorption by phytoplankton pigments, detritus, and colored dissolved organic matter (CDOM). Regions in close proximity to the MARB discharge, R1 and R4, were the locations where $Kd_{490-PAR}$ was most strongly influenced by river discharge and NOx loading (Tables 2 and 3). Nitrogen loading was the dominant variable controlling phytoplankton variability and discharge was the dominant variable controlling detritus and CDOM variability near the river output locations (Green & Gould, 2008; Green et al., 2008).

Fig. 9. Ten-year monthly averages for every other month within the LCS 70 m isobath that has less than or equal to the % PAR at the SWI.

Table 4
Average K_d for the May to July time period for each region. The 30% NOx reduction, 50% NOx reduction, 20% NOx increase, and 20% Q increase are scenarios that were evaluated as to their effect on K_d. Based on these scenarios, for each region the K_d was predicted using the multiple regression models. Shown are the average percentage changes in predicted Kd from the average K_d.

	Average Kd	30% NOx reduction	50% NOx reduction	20% NOx increase	20% Q increase
Region 1	1.65	0%	0%	0%	6%
Region 2	0.72	−6%	−11%	5%	6%
Region 3	0.45	−7%	−12%	5%	6%
Region 4	0.52	−11%	−18%	7%	13%
Region 5	0.15	−5%	−8%	3%	0%

Nutrient and discharge rates peaked in March, April and May. The increased nutrient availability and calm winds in during June, July and August allowed for water column stabilization and phytoplankton biomass to accumulate, therefore absorbing more PAR, thus increasing $Kd_{490-PAR}$ during the summer months. While phytoplankton absorption contributed to $Kd_{490-PAR}$ along the LCS coastal waters, $Kd_{490-PAR}$ along the coast in R1, R2, and R4 was dominated by CDOM absorption, which decreased with increasing salinity (D'Sa & Miller, 2003; Green et al., 2008). The dominant CDOM absorption signature and influence of river discharge in MARB proximal regions suggested $Kd_{490-PAR}$ was controlled not only by phytoplankton responses to nutrients, but also to increased CDOM concentrations.

Regions 2, 3, and 5 $Kd_{490-PAR}$ were more positively correlated with wind speed from October through March. Wind speed was the strongest predictor for detritus, while discharge and wind direction were predictors of CDOM (Green et al., 2008). Green et al. (2008) examined the detritus and CDOM absorption components in relation to wind and discharge, but it was not discussed how these terms contributed to total diffuse light attenuation. Higher wind speeds increased vertical mixing and detritus retention in the water column increasing $Kd_{490-PAR}$ (Salisbury et al., 2004). As river waters spread across the LCS it delivers detritus that rapidly sinks below the pycnocline. Summertime low wind speed and solar heating enhanced the buoyancy of plume waters and detritus was maintained in the surface layers (Walker et al., 1994).

Winds were predominantly from the east except during June, July, and August when they switched to southwest. The east winds produced downwelling conditions along the LCS and the dominant current direction was to the west. Southwest winds promoted upwelling conditions (Hetland & DiMarco, 2008). The change to offshore currents and upwelling conditions may transport MARB surface water onto the LCS, and may also increase the phytoplankton biomass and pigment absorption in areas such as R3 and R5.

The $Kd_{490-PAR}$ of R3 was similar to R4 (Fig. 6A), which was proximal to a MARB river output. These two regions were typical locations of summer hypoxia on the LCS. The distinction between the two regions was the percent surface PAR which reached the SWI due to a difference in bathymetry. R4 and R3 average depths were 28.4 and 14.5 m (Table 1). During non-summer months LCS current direction was to the west which advected Mississippi River discharge over R3 and downwelling conditions limited Atchafalaya discharge from penetrating further onto the LCS. As the summer winds shifted the Atchafalaya plume was transported eastward toward R3 and R5. This pattern was supported by Fig. 8 where the SWI in R3 received less than 0.1% surface PAR (purple and black) October (Fig. 8J) through March (Fig. 8C) and less than 1% surface PAR (green) April (Fig. 8D) through September (Fig. 8I).

Further south on the LCS, R5 PAR at the SWI was greater than 1% surface irradiance (yellow and red) and extended to 91.5°W in May (Fig. 8E) and June (Fig. 8F), but was limited west of 93.0°W in July (Fig. 8G) and never regained the maximal extent by the end of the year (Fig. 8H through 8L). Therefore an increase in $Kd_{490-PAR}$ during June and July resulted from increased phytoplankton biomass due to maximal nutrients, discharge, and water column stabilization; in addition to CDOM and detritus advection onto the LCS due to changing winds and the development of an offshore current.

4.3. Implications for primary production and hypoxia

Previous studies have suggested the importance of light in regulating sub-pycnocline oxygen dynamics (Bierman et al., 1994; Lehrter et al., 2009). This study supports the linkage between the spatial extent of hypoxia, both vertically (Fig. 7A) and horizontally (Fig. 7B), and were correlated to $Kd_{490-PAR}$ along with environmental factors such as river discharge, nutrients, and wind speed. Changes in $Kd_{490-PAR}$ affect sub-pycnocline organic matter production and the

primary production to respiration ratio (P:R), which determined the net gain or loss of oxygen. The use of a constant threshold of 1% surface light for phytoplankton (Kirk, 1994) or 0.1% surface light for MPB compensation depths (Cahoon, 1999) was a suggested indication of light levels that support primary production and hence, oxygen production. Empirical results from this study demonstrated that the 1% euphotic depth was significantly correlated to the depth of hypoxia (Fig. 7). Therefore, a euphotic water column and SWI with at least 0.1% surface irradiance had the potential for net oxygen production (Gattuso et al., 2006; Glud et al., 2002). Thus, low $Kd_{490-PAR}$ may promote sub-pycnocline production and partially offset oxygen depletion by respiration below the pycnocline. When $Kd_{490-PAR}$ increased, the sub-pycnocline P:R ratio decreased and the net drawdown of oxygen proceeded more rapidly.

The increased $Kd_{490-PAR}$ from May to July (Fig. 6) coincided with peak stratification strength, thus limiting the exchange of oxygen across the pycnocline. There were two implications of this temporal pattern as regards hypoxia. First, there was the potential for large sub-pycnocline primary production of organic matter from April to May. The organic matter produced in these waters may be an important substrate for respiration leading to the development of hypoxia. Second, the increased $Kd_{490-PAR}$ from June to July (Fig. 6) would result in decreased sub-pycnocline primary production. Thus, variation in $Kd_{490-PAR}$ (Figs. 7 and 8) may shift the sub-pycnocline metabolism from net oxygen production to net oxygen loss. Eutrophication and physical processes such as stratification and wind mixing events primarily control the extent of hypoxia, while light may partially control the P:R ratio in the sub-pycnocline water column and at the SWI. In this manner, light may play a critical role in structuring the ratio of net community photosynthesis and respiration, which in turn influences the timing and extent of hypoxic water mass formation.

4.4. Future perspective

Nutrient management scenarios of 30 and 50% reductions in nitrogen had the greatest impact on R4 and R3. It could be expected that R4 $Kd_{490-PAR}$ would have the greatest percentage change due to the close proximity of the Mississippi River, but it was surprising that R3 was the second largest percentage change. R1 and R2 were closer in proximity to the Atchafalaya River discharge source, but had no response or smaller decreases in $Kd4_{90-PAR}$ relative to R3. Global climate change scenarios (Table 4) reported by Miller and Russell (1992) and Wolock and McCabe (1999) suggested a 20% increase in MARB discharge. Increased discharge and nitrogen from fertilizer utilization also increased nitrogen export to the LCS (Donner & Scavia, 2007; Donner et al., 2002). MARB discharge was suggested to increase over the last 5 decades (Dai et al., 2009), and forecasted general circulation model results suggested discharge will continue to increase (Nijssen et al., 2001). Increased discharge may increase diffuse attenuation by increasing the supply of nitrogen, phytoplankton biomass, CDOM, and detritus. A decrease in available sub-pycnocline light may subsequently change the balance of P:R and act in a synergistic fashion to increase the area and severity of hypoxia in R2, R3, and R4.

5. Conclusions

The SeaWiFS daily integrated surface PAR was validated and the Kd_{490} diffuse attenuation product was adjusted using the slope and intercept of the regression against field observations of Kd_{PAR}. At the interannual scale, monthly patterns in $Kd_{490-PAR}$ were strongly correlated with wind speed. However, $Kd_{490-PAR}$ was related to MARB discharge and nutrients during the late spring and summer. Increases in $Kd_{490-PAR}$ during June and July were likely the result of increased phytoplankton biomass due to maximal nutrients, discharge, and water column stabilization. In addition, seasonal dynamics of CDOM and detritus may vary with changes in wind patterns. There was potential

for sub-pycnocline primary production during April to May. $Kd_{490-PAR}$ increased from May to July, which may shift the sub-pycnocline metabolism from net autotrophic to net heterotrophic, thus potentially influencing the onset of hypoxia. The availability of light is one of many environmental variables that interact to cause hypoxia. This paper provides, for the first time, an analysis of light availability across the large area of the LCS. Our study was also the first to show that, in addition other factors such as stratification, river discharge, and nutrients, the vertical distribution of hypoxia in the water column was related to the euphotic depth and the horizontal extent of hypoxia was also related to the change in $Kd_{490-PAR}$. Finally, global climate change scenarios suggest $Kd_{490-PAR}$ may increase across the LCS potentially increasing the hypoxic area and shoaling the depth at which the water column turned hypoxic.

Acknowledgments

References

Arnone, R. A., Martinolich, P. M., Gould, R. W., Sydor, M., Stumpf, R. P., & Ladner, S. (1998). Coastal optical properties using SeaWiFS. *Ocean optics XIV*. HA: Kona.

Bailey, S. W., & Werdell, P. J. (2006). A multi-sensor approach for the orbit validation of ocean color satellite data products. *Remote Sensing of Environment, 102*, 12–23.

Baith, K., Lindsay, R., Fu, G., & McClain, C. R. (2001). SeaDAS: Data analysis system developed for ocean color satellite sensors. *EOS, Transactions, American Geophysical Union, 82*.

Bierman, V. J., Hinz, S. C., Wiseman, W. J., Rabalais, N. N., & Turner, R. E. (1994). A preliminary mass balance model of primary productivity and dissolved oxygen in the Mississippi River plume/inner Gulf Shelf region. *Estuaries, 17*, 886–899.

Cahoon, L. B. (1999). The role of benthic microalgae neritic ecosystems. *Oceanography and Marine Biology, 37*, 47–86.

Dai, A. G., Qian, T. T., Trenberth, K. E., & Milliman, J. D. (2009). Changes in continental freshwater discharge from 1948 to 2004. *Journal of Climate, 22*, 2773–2792.

Dale, V. H., Kling, C. L., Meyer, J. L., Sanders, J., Stallworth, H., Armitage, T., et al. (2010). *Hypoxia in the Northern Gulf of Mexica.* New York: Springer.

Donner, S. D., Coe, M. T., Lenters, J. D., Twine, T. E., & Foley, J. A. (2002). Modeling the impact of hydrological changes on nitrate transport in the Mississippi River Basin from 1955 to 1994. *Global Biogeochemical Cycles, 16*, doi:10.1029/2001GB001396.

Donner, S. D., & Scavia, D. (2007). How climate controls the flux of nitrogen by the Mississippi River and the development of hypoxia in the Gulf of Mexico. *Limnology and Oceonography [Limnol. Oceanogr.], 52*, 856–861.

Dortch, Q., Rabalais, N. N., Turner, R. E., & Rowe, G. T. (1994). Respiration rates and hypoxia on the Louisiana shelf. *Estuaries, 17*, 862–872.

D'Sa, E. J., & Miller, R. L. (2003). Bio-optical properties in waters influenced by the Mississippi River during low flow conditions. *Remote Sensing of Environment, 84*, 538–549.

Eadie, B. J., McKee, B. A., Lansing, M. B., Robbins, J. A., Metz, S., & Trefry, J. H. (1994). Records of nutrient-enhanced coastal productivity in sediments from the Louisiana continental shelf. *Estuaries, 17*, 754–765.

Feldman, G. C., & McClain, C. R. (2008). Ocean Color Web, SeaWiFS reprocessing 5.2. In N. Kuring, & S. W. Bailey (Eds.), *NASA Goddard Space Flight Center* http://oceancolor.gsfc.nasa.gov/

Frouin, R., Franz, B., & Werdall, P. J. (2003). The SeaWiFS PAR product. In S. B. Hooker, & E. R. Firestone (Eds.), *SeaWiFS postlaunch technical report series* (pp. 46–50). (Algorithm Updates for the Fourth SeaWiFS Data Reprocessing: NASA Technical Memorandum).

Frouin, R., Franz, B. A., & Werdell, P. J. (2003). The SeaWiFS PAR product. In S. B. Hooker, & E. R. Firestone (Eds.), *SeaWiFS postlaunch technical report series* (pp. 46–50). (Algorithm Updates for the Fourth SeaWiFS Data Reprocessing).

Gattuso, J. P., Gentili, B., Duarte, C. M., Kleypas, J. A., Middelburg, J. J., & Antoine, D. (2006). Light availability in the coastal ocean: Impact on the distribution of benthic photosynthetic organisms and their contribution to primary production. *Biogeosciences, 3*, 489–513.

Glud, R. N., Kuhl, M., Wenzhofer, F., & Rysgaard, S. (2002). Benthic diatoms of a high Arctic fjord (Young Sound, NE Greenland): Importance for ecosystem primary production. *Marine Ecology-Progress Series, 238*, 15–29.

Goolsby, D. A., Battaglin, W. A., Aulenbach, B. T., & Hooper, R. P. (2001). Nitrogen input to the Gulf of Mexico. *Journal of Environmental Quality, 30*, 329–336.

Green, R. E., & Gould, R. W. (2008). A predictive model for satellite-derived phytoplankton absorption over the Louisiana shelf hypoxic zone: Effects of nutrients and physical forcing. *Journal of Geophysical Research, 113*, doi:10.1029/2007JC004594.

Green, R. E., Gould, R. W., & Ko, D. S. (2008). Statistical models for sediment/detritus and dissolved absorption in coastal waters of the northern Gulf of Mexico. *Continental Shelf Research, 28*, 1273–1285.

Greene, R. E., Lehrter, J. C., & Hagy, J. D. (2009). Multiple regression models for hindcasting and forecasting midsummer hypoxia in the Gulf of Mexico. *Ecological Applications, 19*, 1161–1175.

Hetland, R. D., & DiMarco, S. F. (2008). How does the character of oxygen demand control the structure of hypoxia on the Texas–Louisiana continental shelf? *Journal of Marine Systems, 70*, 49–62.

Jahnke, R. A., Nelson, J. R., Richards, M. E., Robertson, C. Y., Rao, A. M. F., & Jahnke, D. B. (2008). Benthic primary productivity on the Georgia midcontinental shelf: Benthic flux measurements and high-resolution, continuous in situ PAR records. *Journal of Geophysical Research, 113*, doi:10.1029/2008JC004745.

JPL (2001). QuickScat science data product user's manual: Overview and geophysical data products. *Publ. D-18053, Pasadena, California*.

Justic, D., Rabalais, N. N., & Turner, R. E. (1996). Effects of climate change on hypoxia in coastal waters: Doubled CO_2 scenario for the northern Gulf of Mexico. *Limnology and Oceanography, 41*, 992–1003.

Kirk, J. T. O. (1994). *Light and photosynthesis in aquatic ecosystems.* New York: Cambridge University Press.

Kleinbaum, D. G., Kupper, L. L., & Muller, K. E. (1986). *Applied regression analysis and other multivariable methods.* Boston: PWS-Kent Publishing.

Laws, E. A., & Archie, J. W. (1981). Appropriate use of regression analysis in marine biology. *Marine Biology, 65*, 13–16.

Lee, Z. -P., Darecki, M., Carder, K. L., Davis, C. O., Stramski, D., & Rhea, W. J. (2005). Diffuse attenuation coefficient of downwelling irradiance: An evaluation of remote sensing methods. *Journal of Geophysical Research, 110*, doi:10.1029/2004JC002573.

Lehrter, J. C., Kurtz, J. C., & Murrell, M. C. (2009). Interactions between Mississippi River inputs, light, phytoplankton biomass, and phytoplankton production on the Louisiana Continental Shelf. *Continental Shelf Research, 29*, 1861–1872.

Lohrenz, S. E., Fahnenstiel, G. L., Kirkpatrick, G. J., Carroll, C. L., & Kelly, K. A. (1999). Microphotometric assessment of spectral absorption and its potential application for characterization of harmful algal species. *Journal of Phycology, 35*, 1438–1446.

Lohrenz, S. E., Fahnenstiel, G. A., Redalje, D. G., Lang, G. A., Chen, X., & Dagg, M. J. (1997). Variations in primary production of northern Gulf of Mexico continental shelf waters linked to nutrient inputs from the Mississippi River. *Marine Ecology Progress Series, 155*, 45–54.

Lohrenz, S. E., Redalje, D. G., Cai, W. -J., Acker, J., & Dagg, M. J. (2008). A retrospective analysis of nutrients and phytoplankton productivity in the Mississippi River plume. *Continental Shelf Research, 28*, 1466–1475.

Lugo-Fernandez, A., Gravois, M., & Montgomery, T. (2008). Analysis of secchi depths and light attenuation coefficients in the Louisiana–Texas shelf, northern Gulf of Mexico. *Gulf of Mexico Science, 1*, 14–27.

Martinolich, P. M. (2005). Automated processing system user's guide v.3.4., Naval Research Laboratory. Washington, D.C. www7333.nrlssc.navy.mil/docs/aps_v3.4/user/aps/

Miller, J. R., & Russell, G. L. (1992). The impact of global warming on river discharge. *Journal of Geophysical Research, 97*, 2757–2764.

Mississippi River/Gulf of Mexico Watershed Nutrient Task Force (2001). Action plan for reducing, mitigating, and controlling hypoxia in the Northern Gulf of Mexico. Washington, DC.

Mississippi River/Gulf of Mexico Watershed Nutrient Task Force (2008). Gulf hypoxia action plan 2008 for reducing, mitigating, and controlling hypoxia in the Northern Gulf of Mexico and improving water quality in the Mississippi River Basin. Washington, DC.

Nijssen, B., O'Donnell, G. M., Hamlet, A. F., & Lettenmaier, D. P. (2001). Hydrologic sensitivity of global rivers to climate change. *Climate Change, 50*, 143–175.

Rabalais, N. N., Atilla, N., Normandeau, C., & Turner, R. E. (2004). Ecosystem history of Mississippi River-influenced continental shelf revealed through preserved phytoplankton pigments. *Marine Pollution Bulletin, 49*, 537–547.

Rabalais, N. N., Turner, R. E., Gupta, B. K. S., Platon, E., & Parsons, M. L. (2007). Sediments tell the history of eutrophication and hypoxia in the northern Gulf of Mexico. *Ecological Applications, 17*, S129–S143.

Redalje, D. G., Lohrenz, S. E., & Fahnenstiel, G. L. (1994). The relationship between primary production and the vertical export of particulate organic matter in a river impacted coastal ecosystem. *Estuaries, 17*, 829–838.

Salisbury, J. E., Campbell, J. W., Linder, E., Meeker, L. D., Muller-Karger, F. E., & Vorosmarty, C. J. (2004). On the seasonal correlation of surface particle fields with wind stress and Mississippi discharge in the northern Gulf of Mexico. *Deep-Sea Research II, 51*, 1187–1203.

Scavia, D., Rabalais, N. N., Turner, R. E., Justic, D., & Wiseman, W. J., Jr. (2003). Predicting the response of Gulf of Mexico hypoxia to variations in Mississippi River nitrogen load. *Limnology and Oceanography, 48*, 951–956.

Stumpf, R. P., Arnone, R. A., Gould, R. W., Martinolich, P., & Ransibrahmanakul, V. (2003). A partially-coupled ocean–atmosphere model for retrieval of water-leaving radiance from SeaWiFS in coastal waters. In S. B. Hooker (Ed.), *Algorithm Updates for the Fourth SeaWiFS Data Reprocessing* (pp. 51–59). : NASA Technical Memo.

Turner, R. E., Milan, C. S., & Rabalais, N. N. (2004). A retrospective analysis of trace metals, C, N, and diatom remnants in sediments from the Mississippi River delta shelf. *Marine Pollution Bulletin, 49*, 548–556.

Turner, R. E., & Rabalais, N. N. (1991). Changes in the Mississippi River quality in this century. *BioSci, 41*, 140–147.

Walker, N. D., Fargion, G. S., Rouse, L. J., & Biggs, D. C. (1994). The great flood of summer 1993: Mississippi River discharge studied. *EOS, Transactions, 75*(409), 414–415.

Wolock, D. M., & McCabe, G. J. (1999). Estimates of runoff using water-balance and atmospheric general circulation models. *Journol of the American Woter Resources Associotion, 35*, 1341–1350.

Wysocki, L. A., Bianchi, T. S., Powell, R. T., & Reuss, N. (2006). Spatial variability in the coupling of organic carbon, nutrients, and phytoplankton pigments in surface waters and sediments of the Mississippi River plume. *Estuorine, Coastol ond Shelf Science, 69*, 47–63.